

Provided for non-commercial research and education use.  
Not for reproduction, distribution or commercial use.



This article appeared in a journal published by Elsevier. The attached copy is furnished to the author for internal non-commercial research and education use, including for instruction at the authors institution and sharing with colleagues.

Other uses, including reproduction and distribution, or selling or licensing copies, or posting to personal, institutional or third party websites are prohibited.

In most cases authors are permitted to post their version of the article (e.g. in Word or Tex form) to their personal website or institutional repository. Authors requiring further information regarding Elsevier's archiving and manuscript policies are encouraged to visit:

<http://www.elsevier.com/copyright>



Contents lists available at ScienceDirect

## Journal of Nuclear Materials

journal homepage: [www.elsevier.com/locate/jnucmat](http://www.elsevier.com/locate/jnucmat)

# Stability and mobility of Cu–vacancy clusters in Fe–Cu alloys: A computational study based on the use of artificial neural networks for energy barrier calculations

M.I. Pascuet<sup>a</sup>, N. Castin<sup>b,c</sup>, C.S. Becquart<sup>d</sup>, L. Malerba<sup>b,\*</sup>

<sup>a</sup> CONICET, Avda. Rivadavia 1917, (1033) Buenos Aires, Argentina

<sup>b</sup> Structural Materials Group, Nuclear Materials Science Institute, Studiecentrum voor Kernenergie (Centre d'Etude de l'Energie Nucléaire (SCK-CEN), Boeretang 200, (2400) Mol, Belgium

<sup>c</sup> Physique des Solides Irradiés et des Nanostructures (PSIN), Université Libre de Bruxelles, Boulevard du Triomphe CP234, (1050) Brussels, Belgium

<sup>d</sup> Laboratoire de Métallurgie Physique et Génie des Matériaux, UMR 8517, Université Lille-1, F-59655 Villeneuve d'Ascq Cédex, France

## ARTICLE INFO

## Article history:

Received 2 December 2009

Accepted 15 February 2011

Available online 21 February 2011

## ABSTRACT

An atomistic kinetic Monte Carlo (AKMC) method has been applied to study the stability and mobility of copper–vacancy clusters in Fe. This information, which cannot be obtained directly from experimental measurements, is needed to parameterise models describing the nanostructure evolution under irradiation of Fe alloys (e.g. model alloys for reactor pressure vessel steels). The physical reliability of the AKMC method has been improved by employing artificial intelligence techniques for the regression of the activation energies required by the model as input. These energies are calculated allowing for the effects of local chemistry and relaxation, using an interatomic potential fitted to reproduce them as accurately as possible and the nudged-elastic-band method. The model validation was based on comparison with available *ab initio* calculations for verification of the used cohesive model, as well as with other models and theories.

© 2011 Elsevier B.V. All rights reserved.

## 1. Introduction

The formation of copper-rich precipitates under irradiation is accepted to be among the main causes of hardening and embrittlement of reactor pressure vessel (RPV) steels during operation, because they act as obstacles to the motion of the dislocations [1]. Positron annihilation studies on FeCu model alloys show that these precipitates are likely to contain a considerable amount of vacancies and to be formed as a result of the diffusion of mobile complexes containing both Cu atoms and vacancies [2–4] (henceforth Cu–vacancy clusters). Consistently, Cu–vacancy clusters are predicted to be relatively stable by *ab initio* calculations [5], supporting the idea that these clusters should be able to migrate as a whole. This contention has been also qualitatively proven by performing high temperature molecular dynamics studies [6]. Thus, models describing Cu precipitation under irradiation should explicitly include a mechanism of formation based on the diffusion of Cu–vacancy clusters.

Kinetic Monte Carlo (KMC) models based on the residence time algorithm [7,8] are suitable to simulate precipitation and also segregation processes [9,10], in acceptable trade-off between accuracy and computing time [11]. Two main classes of KMC models have

been used to describe Cu precipitation under thermal ageing and irradiation: “atomistic” KMC (AKMC) models [12–20] and “object” KMC (OKMC) models [14,21]. In OKMC simulations point-defects, point-defect clusters and mixed clusters are treated without including the detail of their atomic-level configuration and the technique is suitable to simulate irradiation processes in a fairly realistic way, up to a timeframe of years. However, an OKMC model requires as an input the knowledge of all the parameters defining the mobility and stability of the objects included in it. Notably, in order to introduce the mechanism of formation of Cu precipitates via migration of small Cu–vacancy clusters, the diffusion coefficients of these clusters must be known in advance. These are not quantities that can be experimentally measured, though. Obtaining them from *ab initio* calculations, although *a priori* possible by calculating all migration energies for all relevant migration paths, is a very heavy task, which can only be applied in a few simple cases. Molecular dynamics simulations with interatomic potentials could in principle be a solution, but are in practice not applicable, because of the relatively slow migration of vacancies. Either very high temperatures must be simulated (e.g. [6]), thereby making the trajectory of the clusters too short to be statistically significant with a view to deriving their diffusion coefficient from standard techniques [22], or unaffordably long simulations would be required. In contrast, AKMC models spontaneously treat the diffusion of clusters containing solute atoms and point-defects in terms of

\* Corresponding author. Tel.: +32 14 333090; fax: +32 14 321216.

E-mail address: [lmalerba@sckcen.be](mailto:lmalerba@sckcen.be) (L. Malerba).

migration jumps of single point-defects on an atomic lattice. In these models each timestep corresponds to a point-defect jump, so the calculation becomes computationally affordable, allowing a precise determination of trajectories and extraction of diffusivity data, with very good statistics. Given the migration energies and the diffusion mechanism, the model automatically explores all possible migration paths. Thus, the AKMC method is the most suitable to estimate the diffusion coefficients of Cu–vacancy clusters, thereby allowing the parameters for OKMC simulations to be produced. The main shortcoming resides in the fact that entropic effects on the migration barriers are not taken into account, although other entropic contributions, such as configurational entropy, are inherently included in the model.

The application of the AKMC algorithm requires the *a priori* knowledge of the migration energies of, in this case, a vacancy, as a function of the local atomic environment (LAE), which varies because Cu atoms and other vacancies are in each case differently distributed around it. These energies are customarily estimated using heuristic approaches, such as linear relationships with the total energy variation between before and after the jump [12–14,17,18,20], or broken bond methods limited to bonds with the first and second nearest neighbour shell [9,10,15–16,19]. However, these approaches are insufficient to describe reliably the complexity of the dependence of the activation energies for a vacancy jump on the LAE, as shown for example in [23].

In [24] the problem was solved by pre-calculating, with a suitable interatomic potential [25,26], all the energy barriers corresponding to all possible LAEs encountered during migration by the vacancies in the Cu–vacancy cluster (limited, however, to the 3rd nearest neighbour shell) and by storing them in tables. This is indeed doable if the LAEs are limited to a sufficiently small amount of atoms and, in general, if the total number of LAEs remains reasonably small. In such a case, the production of the tables requires a long, though still affordable, amount of computing time, but then fast search algorithms can find rapidly the proper value in the tables during the AKMC simulations.

In this work, we want to improve the reliability of the same type of calculations performed in [24], by taking into account the effect on the migration energy of a LAE more extended than the 3rd nearest neighbour (3nn) shell. We also want to study larger clusters, for which the tabulation of all possible barriers for all possible LAEs is unfeasible. In order to do this, we resort to the method developed in [23,27], in which a properly trained artificial neural network (ANN) is used to calculate, on-demand and on-the-fly, during the AKMC simulation, the migration energies as functions of the LAEs.

The paper is organised as follows. In Section 2 we summarise the fundamentals of our artificial neural network-based AKMC simulation. In Section 3 we present our results for a number of Cu–vacancy clusters. In the first place, we provide the statically-calculated formation and binding energies, as these are the quantities traditionally used in OKMC simulations to estimate stability parameters [21]. The calculations are performed using the same interatomic potential as employed for the energy barrier calculations and the results are compared with *ab initio* calculations, in order to assess the reliability of the potential. Then we apply the previously-sketched AKMC method to study mobility and stability of small clusters (up to six elements) versus temperature. Whenever possible, we compare our results with previous ones, obtained in [24]. Subsequently, we present some results on the diffusivity of large copper clusters, containing up to 150 atoms and only one vacancy, and compare the diffusion coefficients obtained with those estimated with other methods. Finally, in Section 4 we analyse and discuss the reliability of the use of the ANN to replace a tabulation of rigorously calculated migration energy values, as well as, more generally, the reliability of the results obtained.

## 2. Computational model

### 2.1. The AKMC algorithm and the problem of the evaluation of energy barriers

According to standard transition state theory, the frequency of a thermally activated event, such as a vacancy jump  $j$  in an alloy, can be expressed as:

$$\Gamma_j = \nu \exp(-E_j/k_B T) \quad (1)$$

where  $\nu$  is an attempt frequency, that can be considered constant in first approximation (on the order of the Debye frequency; here  $\nu = 6 \times 10^{12} \text{ s}^{-1}$ ),  $k_B$  is Boltzmann's constant,  $T$  the absolute temperature and  $E_j$  the LAE-dependent activation energy of the jump (denoted here as energy barrier, or migration energy). These frequencies are used in an AKMC framework to assign a probability to all possible vacancy migration events: the 1nn migration of vacancies, one at a time. The simulation time is incremented following the mean residence time algorithm [7,8].

Given a suitable interatomic potential (e.g. [25,26] for the Fe–Cu alloy), the energy barriers can be rigorously calculated, for any LAE, using the nudged-elastic-band (NEB) method [28]. Atomic-level techniques of this type take implicitly into consideration the influence of the nature of the surrounding atoms on the vacancy jump barrier, as well as strain field effects. However, the use of a NEB calculation at each AKMC timestep to evaluate all  $\Gamma_j$  from Eq. (1) would require a prohibitively long CPU time. As anticipated in the introduction, when the total number of LAEs to be considered is reduced, the production of tables of energy barriers for all possible cases, to be fed to the AKMC code, is possible (e.g. [24]). However, if the clusters to be studied are not-so-small, the size of the table to be constructed grows very fast. In these cases, the only alternative to tabulating is to find patterns in the dependence of the energy barriers on the LAE and use a model instead of tables. For this purpose, we resorted to an artificial intelligence method [27].

### 2.2. Artificial neural network as regression tool for energy barrier calculation

ANNs are considered as universal approximation tools, capable of learning from experience and to find non-evident dependencies between data. In this work, they are used as a very fast and powerful numerical regression method that can reproduce the complex relation existing between the vacancy migration energy and the LAE. We use ANN of the feed-forward multilayer perceptron type, with one hidden layer, using linear combination functions and sigmoidal non-linear activation functions [27].

The development of an ANN requires first the production of examples, i.e. a table of LAEs and corresponding migration energies calculated with the NEB method. This table must be divided into two non-overlapping sets: a training set and a validation set. The ANN is trained to reproduce the former and validated on the latter, by definition made of examples never seen before by the ANN, i.e. not included in the training set. Given these sets, a complete description of the methodology that is followed in order to design the ANN can be found in [27].

Fig. 1 shows the accuracy reached by the ANN after training, when up to seven Cu atoms and seven vacancies are included in the LAE (FeCuVac system). The LAE encompasses the 5th shell of nearest neighbours around the migrating vacancy and its destination (5nn approximation). The mean relative error is in this case 5.67%, and the correlation factor  $R^2$  is 0.95. The mean bias,  $\sum(O - d)/N$ , is 0.0024 eV and the mean error,  $\sum|O - d|/N$ , is 0.033 eV ( $O$  is the ANN output,  $d$  the desired target, and  $N$  the number of points). The correlation is globally good, although not perfect, because ANN predictions and NEB calculated barriers do

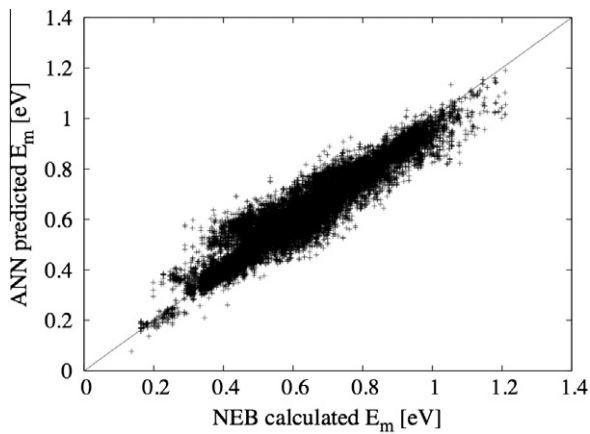


Fig. 1. Predictive capability of the ANN developed for the FeCuVac system (seven Cu atoms and seven vacancies max.), with the LAE extended to 5nn shell, as compared with NEB calculated values from the validation set.

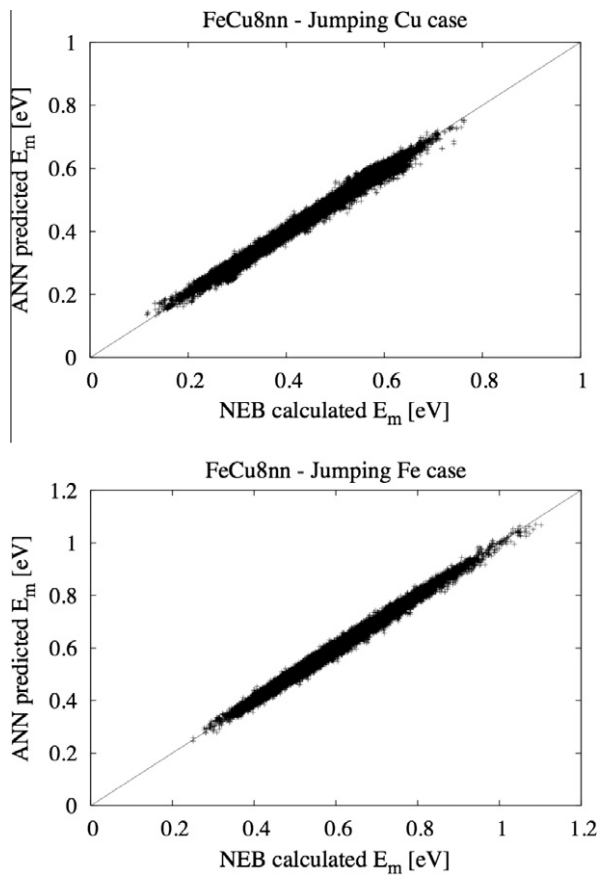


Fig. 2. Predictive capability of the ANN developed for the FeCu system, with LAE extended up to 8nn shell: upper panel, case of a migrating Cu atom; lower panel, case of migrating Fe atom.

not always compare one-to-one. As discussed in Section 4, the quality of the performance of this ANN was *a posteriori* observed to vary significantly from cluster to cluster, so that in principle, via proper retraining, its improvement is possible. Nevertheless, in Section 4 it is also shown that, probably due to the absence of significant biases in the error committed by the ANN, the results are globally acceptable when compared with results obtained directly from tabulations.

In the case of the FeCu system (no extra vacancies in the LAE), two separate ANNs were developed, namely, one for cases when

the vacancy exchanges its position with a Cu atom, and another one for exchanges with Fe atoms. The LAE included up to the 8th nearest neighbour shell (8nn approximation). Fig. 2 shows that in this case the ANN accuracy is extremely good for both Cu and Fe migrating atoms. The mean relative error in the migrating Cu case is 1.13% and 1.10% in the migrating Fe case. The correlation factor  $R^2$  and the mean bias are in both cases 0.99 and 0.001 eV, respectively. The mean error is 0.0051 eV for the migrating Cu case and 0.007 eV for the migrating Fe case.

The ANNs of Figs. 1 and 2 were used to assess  $E_j$  in Eq. (1) at each timestep in the AKMC simulations performed to study the diffusivity of, respectively, small Cu–vacancy clusters (FeCuVac system) and Cu clusters containing only one vacancy (FeCu system). The methodology used to extract information from the simulations for the estimation of the diffusion coefficients is described together with the results in the next section.

### 3. Results

#### 3.1. Formation and binding energies of small clusters

The nanostructural features of main interest for the present investigation are the small Cu–vacancy clusters. As a first characterisation of their stability, static calculations of the relevant formation and binding energies have been performed, using the Fe–Cu interatomic potential developed in [25,26]. The latter has been fitted taking care for a correct description of both the thermodynamic properties of the FeCu system (phase diagram, solubility limit especially) and the interaction between Cu atoms and vacancies in Fe. In particular, migration energies of vacancies in presence of Cu atoms were fitted following indications from available *ab initio* calculations, which suggested that Cu atoms would be dragged by vacancies, as a consequence of the formation of Cu–vacancy pairs migrating together as a whole, as observed also in molecular dynamics simulations [6]. The binding energies between Cu atoms and vacancies were fitted targeting the values that were found to provide the best agreement between experiments and AKMC simulations in [17,29]. Here we calculate the formation and binding energies obtained with this Fe–Cu potential and compare them with *ab initio* calculations. The latter were performed with the density functional theory (DFT) code (VASP) [30], within the Generalised Gradient Approximation (GGA) of Perdew and Wang, PW91 [31] and using fully non-local ultra-soft pseudo-potentials (USPP) of the Vanderbilt type [32] to describe electron–ion interaction. The pseudo-potentials were taken from the code library. The supercell approach with periodic boundary conditions was used to simulate point-defects as well as pure phases. Brillouin zone sampling was performed using the Monkhorst and Pack scheme [33]. The plane wave cut-off energy was 240 eV in order to get converged results. 54 atom supercells with 125 k-points as well as 128 atoms with 27 k-points were used to check the convergence of the calculations with supercell size. Only 128 atom results are reported, which are known from previous experience to be already size-converged (i.e. calculations with more atoms would provide the same results).

Formation energies of vacancy clusters, copper clusters and copper–vacancy clusters, respectively, are obtained using the following formulae:

$$\begin{aligned}
 E_f(N_V) &= (N_0 - N_V) \cdot [E_c(N_V \text{ in bcc Fe}) - E_c(\text{bcc Fe})] \\
 E_f(N_{Cu}) &= N_0 \cdot E_c(N_{Cu} \text{ in bcc Fe}) - [(N_0 - N_{Cu}) \cdot E_c(\text{bcc Fe}) \\
 &\quad + N_{Cu} \cdot E_c(\text{fcc Cu})] \\
 E_f(N_V + N_{Cu}) &= (N_0 - N_V) \cdot E_c(N_V + N_{Cu} \text{ in bcc Fe}) \\
 &\quad - [(N_0 - N_{Cu} - N_V) \cdot E_c(\text{bcc Fe}) + N_{Cu} \cdot E_c(\text{fcc Cu})]
 \end{aligned}
 \tag{2}$$

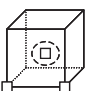
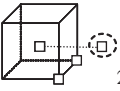
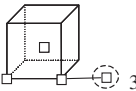
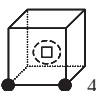
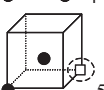
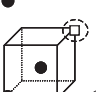
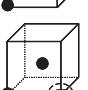
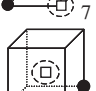
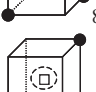


**Table 1**

Formation ( $E_f$ ) and binding ( $E_b$ ) energies of vacancy–vacancy, Cu–Cu and Cu–vacancy pairs at different mutual distances: interatomic potential (IAP) and *ab initio* (DFT-USPP) calculations using 128 atom supercells.

	$E_f$ (eV)		$E_b$ (eV)	
	IAP	DFT-USPP	IAP	DFT-USPP
V	1.71	2.00	–	–
V–V (1nn)	3.30	3.84	0.13	0.16
V–V (2nn)	3.19	3.70	0.24	0.30
V–V (3nn)	3.45	–	–0.02	–0.02
V–V (4nn)	3.39	–	0.03	0.09
Cu	0.43	0.55	–	–
Cu–Cu (1nn)	0.79	0.94	0.08	0.16
Cu–Cu (2nn)	0.79	1.05	0.08	0.05
Cu–Cu (3nn)	0.87	–	~0	~0
Cu–Cu (4nn)	0.87	–	~0	~0
Cu–V (1nn)	2.05	2.39	0.10	0.16
Cu–V (2nn)	2.06	2.34	0.09	0.21
Cu–V (3nn)	2.15	–	~0	–

**Table 2**

Formation and binding energies (eV) for some small Cu–vacancy clusters, as calculated with the interatomic potential and using *ab initio* methods. The enclosed element is the one for whose removal the binding energy is evaluated.

	$E_f$ (eV)		$E_b$ (eV)	
	IAP	IAP	IAP	DFT-USPP
 1	4.62	–	0.28	0.52
 2	5.78	–	0.57	0.70
 3	6.09	–	0.24	0.31
 4	2.31	–	0.19	0.36
 5	2.40	–	0.10	0.22
 6	2.40	–	0.10	0.18
 7	2.31	–	0.18	0.35
 8	2.37	–	0.21	0.42
 9	2.39	–	0.19	0.33
 10	2.69	–	0.08	0.19
 11	2.49	–	0.28	0.46

Here,  $N_0$  is the total amount of atomic lattice sites in the box,  $N_V$  is the number of vacancies in the cluster, and  $N_{Cu}$  is the number of copper atoms in the cluster;  $E_c(N_V$  in bcc Fe) is the relaxed energy

per atom of a bcc Fe matrix containing a cluster of  $N_V$  vacancies in its lowest energy configuration,  $E_c(N_{Cu}$  in bcc Fe) is the same energy for a system containing a cluster of  $N_{Cu}$  copper atoms, and  $E_c(N_V + N_{Cu}$  in bcc Fe) is again the same energy containing a cluster of  $N_V$  vacancies and  $N_{Cu}$  copper atoms; finally,  $E_c(\text{bcc Fe})$  is the cohesive energy of pure bcc Fe and  $E_c(\text{fcc Cu})$  is the cohesive energy of pure fcc Cu. It should be noted that the formation energies in Eq. (2) are independent of the choice of  $N_0$ , provided that the energies per atom of the defective system used in such equation to calculate them correspond to the value of  $N_0$  used in the same equation.

Once the formation energies are known, the binding energy of a vacancy (V) to a cluster of certain size can be obtained according to the following expression:

$$E_b(V) = E_f(\text{cluster}) + E_f(V) - E_f(\text{cluster} + V) \quad (3)$$

where  $E_f(\text{cluster})$  is the formation energy of the cluster,  $E_f(V)$  is the formation energy of the vacancy alone, and  $E_f(\text{cluster} + V)$  is the formation energy of the cluster plus the vacancy.

The results from the interatomic potential and from *ab initio* calculations, for a number of cluster configurations, are given in Tables 1 and 2. In particular, Table 1 shows the formation and binding energies for the Cu–vacancy, Cu–Cu and vacancy–vacancy pairs. Table 2 lists the same quantities for a number of clusters (results obtained with the interatomic potential for more clusters, up to six elements, are reported in [34]). It can be seen that the potential generally underestimates the strength of the Cu–vacancy binding, as compared to DFT data. At the same time, DFT binding energy values for Cu–vacancy pairs could not be used as they were in [17,20,29] in order to provide acceptable results in AKMC

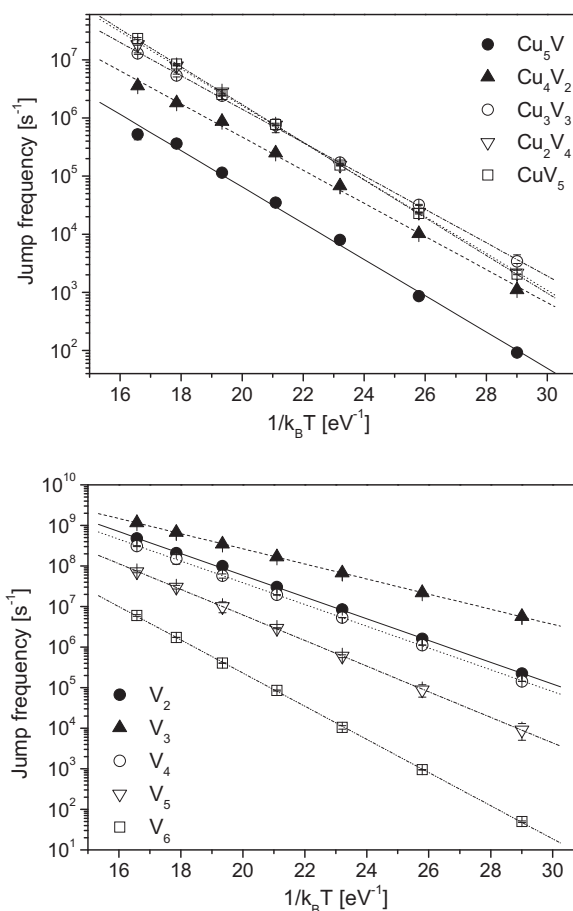


**Fig. 3.** Jump frequencies of Cu–vacancy clusters with six elements (above) and of vacancy clusters (below).



simulations of Cu precipitation in Fe. The potential provides pair binding energies very close to those chosen for the AKMC model we refer to. Thus, the overall performance of the potential can be judged acceptable, although probably biased on the side of underestimating the strength of the Cu–vacancy interaction in Fe. This possible bias will have to be taken into account when discussing the results.

### 3.2. Mobility and stability of small clusters

The mobility and stability of small clusters were investigated using the AKMC model driven by the ANN, described in Section 2. The clusters studied were complexes formed by Cu atoms (Cu) and vacancies (V) up to six elements, namely CuV, CuV<sub>2</sub>, Cu<sub>2</sub>V, Cu<sub>2</sub>V<sub>2</sub>, CuV<sub>3</sub>, Cu<sub>3</sub>V, CuV<sub>4</sub>, Cu<sub>2</sub>V<sub>3</sub>, Cu<sub>3</sub>V<sub>2</sub>, Cu<sub>4</sub>V, CuV<sub>5</sub>, Cu<sub>2</sub>V<sub>4</sub>, Cu<sub>3</sub>V<sub>3</sub>, Cu<sub>4</sub>V<sub>2</sub> and Cu<sub>5</sub>V, as well as vacancy clusters of up to six elements: V<sub>2</sub>, V<sub>3</sub>, V<sub>4</sub>, V<sub>5</sub> and V<sub>6</sub>. The clusters were created in their expected lowest energy configuration at the centre of a box containing an otherwise pure bcc Fe matrix and the system was let to evolve according to the AKMC scheme. The energy barriers were provided in all cases by the FeCuVac ANN, except for the Cu<sub>5</sub>V cluster, for which the FeCu ANNs were used instead. The simulation box contained 20 × 20 × 20 cubic cells, i.e. 16,000 atoms. Following the methodology applied in [24], the mobility was studied at different temperatures, between 400 K and 700 K, by tracing the successive positions of the centre-of-mass of the cluster (arbitrarily and conveniently assigning the same mass to Cu and V). The latter was considered to be a cluster so long as all elements forming it remained at a mutual distance shorter than the 2nn distance: as soon as this condition was not fulfilled any more, the simulation was stopped and the cluster lifetime in the specific simulation was recorded. For each temperature and cluster, 100–300 simulations were performed, in order to have enough statistics (see Fig. 3).

#### 3.2.1. Jump frequencies

From the analysis of the successive positions and the corresponding time, in each series of simulations for a given cluster at temperature *T*, the jump frequency could be deduced, using the equation:

**Table 3**

Attempt frequency (in units of 10<sup>13</sup> s<sup>-1</sup>), migration energy (eV) and 1nn average distance for cluster centre-of-mass jumps (in units of lattice parameter, *a*<sub>0</sub>), for all small clusters studied, as obtained from the jump frequency study. For prefactor and migration energies the error bar is also given.

N	Complex	<i>v</i> <sub>0</sub>		<i>E</i> <sub>m</sub> <sup>v</sup>				Dist
2	V <sub>2</sub>	1.14	±0.18	2.12*	0.62	±0.005	0.62*	0.92
3	V <sub>3</sub>	0.14	±0.01	0.2*	0.43	±0.001	0.49*	0.92
4	V <sub>4</sub>	0.89	±0.05	2.7*	0.62	±0.003	0.72*	0.92
5	V <sub>5</sub>	1.25	±0.08	4.4*	0.72	±0.003	0.88*	0.90
6	V <sub>6</sub>	3.43	±0.04	62.8*	0.94	±0.005	1.11*	0.89
2	CuV	0.61	±0.26	0.95*	0.67	±0.019	0.65*	1.00
3	CuV <sub>2</sub>	0.68	±0.13	1.55*	0.65	±0.008	0.68*	0.94
3	Cu <sub>2</sub> V	0.36	±0.05	1.19*	0.65	±0.007	0.68*	0.94
4	CuV <sub>3</sub>	0.52	±0.10	0.17*	0.64	±0.008	0.55*	0.92
4	Cu <sub>2</sub> V <sub>2</sub>	0.65	±0.05	72.9*	0.69	±0.003	0.86*	0.92
4	Cu <sub>3</sub> V	0.41	±0.01	8.53*	0.71	±0.012	0.78*	0.92
5	CuV <sub>4</sub>	0.601	±0.09		0.71	±0.007		0.90
5	Cu <sub>2</sub> V <sub>3</sub>	0.181	±0.04		0.65	±0.011		0.90
5	Cu <sub>3</sub> V <sub>2</sub>	0.103	±0.03		0.68	±0.012		0.90
5	Cu <sub>4</sub> V	0.007	±0.01		0.67	±0.018		0.90
6	CuV <sub>5</sub>	0.502	±0.06		0.75	±0.005		0.89
6	Cu <sub>2</sub> V <sub>4</sub>	0.367	±0.04		0.73	±0.005		0.89
6	Cu <sub>3</sub> V <sub>3</sub>	0.078	±0.01		0.66	±0.008		0.90
6	Cu <sub>4</sub> V <sub>2</sub>	0.023	±0.01		0.66	±0.015		0.89
6	Cu <sub>5</sub> V	0.011	±0.01		0.72	±0.022		0.90

Data denoted by \* correspond to calculations from [24] and are added for comparison.

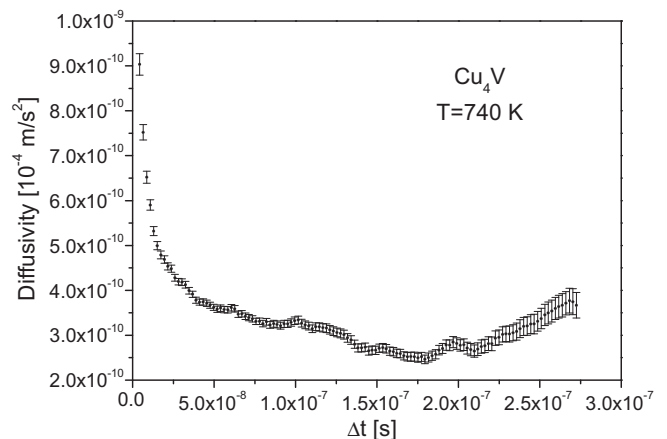


**Fig. 4.** Example of convergence of the diffusion coefficient as a function of the length of the time interval  $\Delta t$  chosen when applying Eq. (7) ( $T = 700$  K, cluster Cu<sub>4</sub>V).

$$v(T) = \frac{1}{N^{sim}} \sum_{i=1}^{N^{sim}} \frac{n_{jumps}^i}{\tau_{life}^i}(T) \quad (4)$$

Here,  $n_{jumps}^i$  is the number of jumps equal to, or larger than, 1nn distance, performed by the centre-of-mass during the lifetime of the cluster,  $\tau_{life}^i$ . The migration energies of the clusters were obtained using classical Arrhenius exponential functions to interpolate the data-points obtained for the different temperatures:

$$v(T) = v_0 \exp(-E_m^v/k_B T) \quad (5)$$

The resulting  $v_0$  and  $E_m^v$  for all studied clusters are given in Table 3. For complexes of up to four elements, our results could be compared with those obtained in [24], where energy barriers were calculated with the same interatomic potential as here, but limited to LAEs extended only to the 3nn distance. For visual illustration, the corresponding Arrhenius plots for six element Cu–vacancy clusters and for all vacancy clusters studied are given in Fig. 3 (all plots for all Cu–vacancy clusters can be found in [34]). In Table 3 we provide also the actual average jump distance for each cluster, in units of lattice parameters. In all cases this distance is longer than the 1nn distance and is as large as the 2nn distance for the CuV cluster.

#### 3.2.2. Diffusion coefficients

The diffusion coefficient can be estimated similarly to the jump frequency using the following equation [24]:

$$D(T) = \frac{1}{N^{sim}} \sum_{i=1}^{N^{sim}} \frac{R_i^2}{6\tau_{life}^i}(T) \quad (6)$$

where  $R_i^2$  is the square of the total displacement of defect *i* during its lifetime. This scheme is similar to the one originally applied by Guinan et al. for the study of the diffusivity of self-interstitials [35] and amply discussed in [22]. The sampled time, however, is here in each case dictated by the cluster lifetime and is therefore not the same for each run. Eq. (6) corresponds in fact to an adaptation of the general Einstein equation [22,36]:

$$D(T) = \frac{\langle R^2 \rangle(T)}{6\Delta t} \quad (7)$$

where  $\langle R^2 \rangle$  is the mean square displacement within the time interval  $\Delta t$  of a population of random walkers. However, as discussed in [22], the accuracy of the estimated diffusivity with adaptations of Eq. (7) is sensitive to the choice of the time interval length. To analyse in each case (each cluster and temperature) the dependence of the diffusion coefficient and its variance versus isochronal sequences, all trajectories that were independently simulated were

eventually chained to one another. The long trajectory thereby obtained was then decomposed into time segments of (approximately) equal length,  $\Delta t$ . The average of the square distances covered by the defect within each interval of length  $\Delta t$  was used

**Table 4**

Diffusivity prefactor (in units of  $10^{-8} \text{ m}^2/\text{s}$ ) and migration energy (eV) for all small clusters studied, including uncertainties, as obtained from the diffusion coefficient study.

N	Complex	$D_0$	$E_m^D$	$E_m^D$	$E_m^D$	$E_m^D$	$E_m^D$
2	$V_2$	22.60	$\pm 6.24$	29.8*	0.63	$\pm 0.012$	0.63*
3	$V_3$	0.21	$\pm 0.07$	1.11*	0.44	$\pm 0.015$	0.46*
4	$V_4$	9.77	$\pm 2.51$	27*	0.62	$\pm 0.011$	0.71*
5	$V_5$	9.76	$\pm 1.80$	45.5*	0.71	$\pm 0.009$	0.88*
6	$V_6$	46.30	$\pm 5.16$	21.6*	0.95	$\pm 0.005$	1.06*
2	$\text{CuV}$	2.78	$\pm 0.73$	4.67*	0.64	$\pm 0.012$	0.63*
3	$\text{CuV}_2$	8.59	$\pm 4.74$	9.76*	0.69	$\pm 0.025$	0.67*
3	$\text{Cu}_2\text{V}$	5.20	$\pm 1.77$	6.7*	0.72	$\pm 0.015$	0.66*
4	$\text{CuV}_3$	2.59	$\pm 0.85$	1.78*	0.65	$\pm 0.015$	0.56*
4	$\text{Cu}_2\text{V}_2$	2.05	$\pm 0.66$	2200*	0.68	$\pm 0.014$	0.89*
4	$\text{Cu}_3\text{V}$	1.89	$\pm 0.96$	65.8*	0.74	$\pm 0.023$	0.77*
5	$\text{CuV}_4$	1.44	$\pm 0.78$		0.67	$\pm 0.024$	
5	$\text{Cu}_2\text{V}_3$	0.69	$\pm 0.36$		0.63	$\pm 0.024$	
5	$\text{Cu}_3\text{V}_2$	0.49	$\pm 0.20$		0.66	$\pm 0.018$	
5	$\text{Cu}_4\text{V}$	0.75	$\pm 0.42$		0.75	$\pm 0.025$	
6	$\text{CuV}_5$	2.08	$\pm 0.82$		0.72	$\pm 0.018$	
6	$\text{Cu}_2\text{V}_4$	0.98	$\pm 0.49$		0.68	$\pm 0.022$	
6	$\text{Cu}_3\text{V}_3$	0.36	$\pm 0.20$		0.64	$\pm 0.024$	
6	$\text{Cu}_4\text{V}_2$	1.09	$\pm 0.38$		0.72	$\pm 0.015$	
6	$\text{Cu}_5\text{V}$	0.71	$\pm 0.45$		0.79	$\pm 0.028$	

Data denoted by \* correspond to calculations from [24] and are added for comparison.

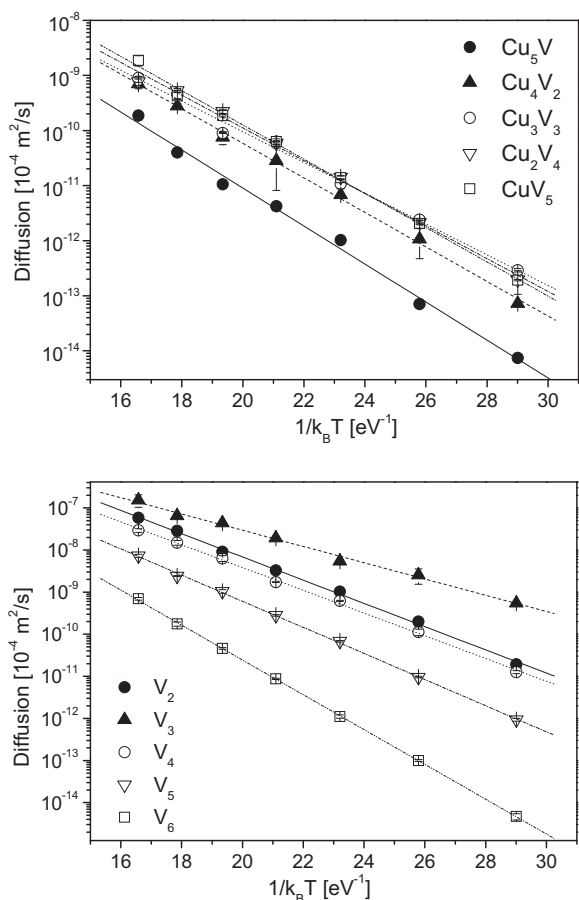


**Fig. 5.** Diffusion coefficients of Cu–vacancy clusters with six elements (above) and of vacancy clusters (below).

to estimate the mean square displacement, which corresponds to the (almost) exact application of the method originally proposed in [35]. By varying  $\Delta t$  in a significantly large interval (possible after chaining trajectories), the converged asymptotical value of the diffusion coefficient is found, as described in what follows.

One example of plot of  $D(\Delta t)$  for  $T = 740 \text{ K}$  and its variance (error bar) is shown in Fig. 4, for the  $\text{Cu}_4\text{V}$  cluster. It can be seen that indeed they depend on the choice of  $\Delta t$ . Short time intervals provide larger statistics, but also larger errors bars, because correlation effects are not correctly sampled. For longer time intervals a convergence to an (almost)  $\Delta t$ -independent  $D$  value is observed, due to a more correct sampling of correlation effects in each interval. However, by choosing too long time intervals, the error bars increase again, because the number of intervals over which the average is taken decreases. Hence, the  $D$  value cannot be simply obtained as the asymptot for large  $\Delta t$ . Instead, it must be a trade-off between correctness of the sampling and accuracy. For each cluster and temperature, therefore, the diffusion coefficient was estimated as the average between the maximum and the minimum value in the convergence zone. The uncertainty in the calculation of the diffusion coefficient was accordingly estimated as the difference between this average and the largest value in this zone.

Finally, in order to estimate the migration energy and the diffusivity prefactor for each cluster, the data-points for different temperatures were interpolated using the Arrhenius expression:

$$D(T) = D_0 \exp(-E_m^D/k_B T) \quad (8)$$

The resulting  $D_0$  and  $E_m^D$  for all studied clusters are provided in Table 4. For complexes up to four elements, the results obtained in [24] are added for comparison. For visual illustration, the corresponding Arrhenius plots for six element Cu–vacancy clusters and for all vacancy clusters studied are given in Fig. 5 (all plots for all Cu–vacancy clusters can be found in [34]).

### 3.2.3. Correlation factors and cluster lifetimes

The migration energy obtained from the diffusion coefficient,  $E_m^D$ , may differ from the homologous value obtained from the jump frequency,  $E_m^v$ , because in the former case correlation effects are naturally allowed for, but not in the latter. These effects are related to jumps or series of jumps that, while accounted for in the determination of the jump frequency via Eq. (4), do not contribute to the diffusion coefficient (e.g. back and forth jumps, or loops in the trajectory). In general, the relationship between diffusion coefficient and jump frequency for three-dimensionally migrating species can be expressed as:

$$D(T) = f_c(T) \frac{v_j(T)\Delta^2}{6} \quad (9)$$

where  $\Delta$  is the jump distance (between 1nn and 2nn distance in the present case) and  $f_c$  is the correlation factor, that carries the above-mentioned effects. This factor can be temperature dependent. In the case of all clusters studied in this work, at any rate, and for all temperatures, the correlation factors are always close to unity [34]. Consistently, the migration energies obtained with the two interpolations are extremely similar.

The dissociation energy,  $E_{dis}$ , and the lifetime prefactor,  $\tau_0$ , were estimated from the temperature dependence of the average lifetime, using the equation:

$$\tau_{life}(T) = \tau_0 \exp(E_{dis}/k_B T) \quad (10)$$

The results for all clusters studied are provided in Table 5. For visual illustration, the corresponding Arrhenius plots for six element Cu–vacancy clusters and for all vacancy clusters studied are given in Fig. 6 (all plots for all Cu–vacancy clusters can be found in [34]).

**Table 5**  
Lifetime prefactor (in units of  $10^{-14}$  s) and dissociation energy (eV) for all small clusters studied, specifying error bars, too.

N	Complex	$\tau_0$	$E_{dis}$	$E_{dis}$	$E_{dis}$	$E_{dis}$	$E_{dis}$
2	V <sub>2</sub>	0.99 ±0.12	0.75*	0.81	±0.007	0.81*	
3	V <sub>3</sub>	1.48 ±0.19	0.98*	0.82	±0.006	0.91*	
4	V <sub>4</sub>	0.39 ±0.07	0.3*	0.97	±0.008	1.08*	
5	V <sub>5</sub>	0.36 ±0.08	0.9*	1.10	±0.010	1.2*	
6	V <sub>6</sub>	0.17 ±0.07	0.04*	1.30	±0.019	1.45*	
2	CuV	8.26 ±0.12	8.3*	0.69	±0.007	0.71*	
3	CuV <sub>2</sub>	0.70 ±0.23	2.45*	0.83	±0.015	0.81*	
3	Cu <sub>2</sub> V	6.53 ±0.16	432*	0.72	±0.011	0.70*	
4	CuV <sub>3</sub>	5.18 ±0.78	2.14*	0.80	±0.007	0.88*	
4	Cu <sub>2</sub> V <sub>2</sub>	1.10 ±0.16	0.65*	0.88	±0.006	0.96*	
4	Cu <sub>3</sub> V	3.16 ±0.91	68.6*	0.83	±0.013	0.81*	
5	CuV <sub>4</sub>	2.65 ±1.24		0.90	±0.021		
5	Cu <sub>2</sub> V <sub>3</sub>	4.37 ±0.95		0.84	±0.009		
5	Cu <sub>3</sub> V <sub>2</sub>	1.76 ±0.50		0.90	±0.012		
5	Cu <sub>4</sub> V	3.45 ±0.92		0.88	±0.011		
6	CuV <sub>5</sub>	3.21 ±1.43		0.96	±0.020		
6	Cu <sub>2</sub> V <sub>4</sub>	3.34 ±0.97		0.92	±0.013		
6	Cu <sub>3</sub> V <sub>3</sub>	5.86 ±2.02		0.86	±0.015		
6	Cu <sub>4</sub> V <sub>2</sub>	3.02 ±0.57		0.90	±0.006		
6	Cu <sub>5</sub> V	0.38 ±0.11		0.98	±0.013		

Data denoted by \* correspond to calculations from [24] and are added for comparison.

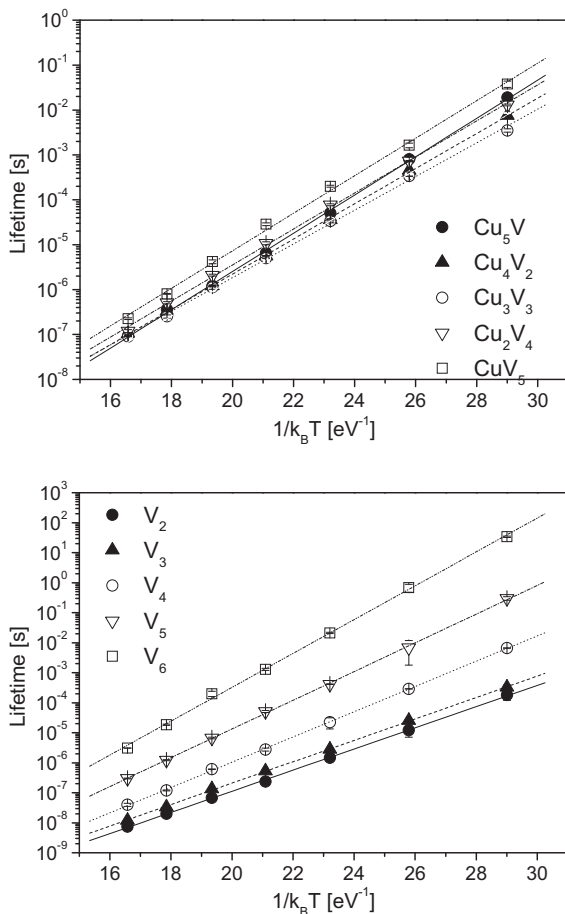


**Fig. 6.** Lifetime of Cu–vacancy clusters with six elements (above) and of vacancy clusters (below).

### 3.3. Mobility of large Cu clusters

Large clusters of 15, 25, 65 and 150 Cu atoms and only one vacancy were created in a  $30 \times 30 \times 30$  cell simulation box, with

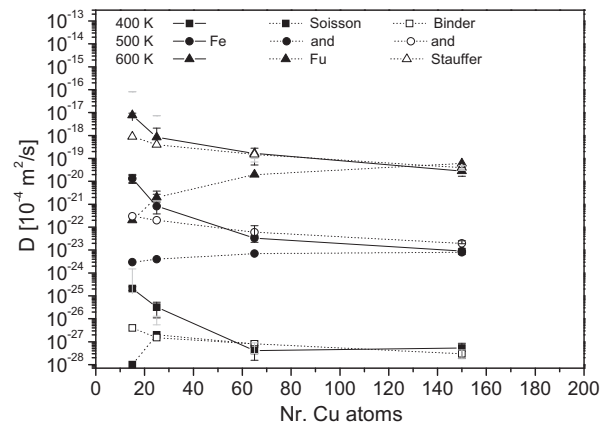


**Fig. 7.** Diffusion coefficient versus number of Cu atoms in precipitates at 400, 500 and 600 K. The solid lines correspond to the present work; dashed lines correspond to the results of [19]; full symbols are AKMC simulations, empty symbols calculations using the Binder–Stauffer model.

a pure bcc Fe matrix. The FeCu-8nn ANNs were used for the calculation of the energy barriers. The mobility was studied by tracing the successive positions of the centre-of-mass of the cluster at three temperatures: 400 K, 500 K and 600 K. The diffusion coefficients were studied in the same way as for small clusters (Section 3.2.2). The results are given in Fig. 7, where the diffusion coefficient versus the number of Cu atoms in the cluster is shown for the three different temperatures studied. Results by Soisson and Fu obtained from similar studies conducted with a different AKMC model [19], and according to a mean-field Binder–Stauffer model [37–39], are shown for comparison on the same graph, after renormalisation. The latter was necessary because the raw diffusivity prefactor values bear a relationship with the chosen constant attempt frequency in Eq. (1):  $\nu_{Fe} = 5 \times 10^{15} \text{ s}^{-1}$  and  $\nu_{Cu} = 2 \times 10^{15} \text{ s}^{-1}$  in [19], while here  $\nu_{Fe} = \nu_{Cu} = 6 \times 10^{12} \text{ s}^{-1}$ . Moreover, in [19] time had been rescaled following the equation:

$$t = t_{MC} \frac{C_V^{MC}(Fe)}{C_V^{eq}(Fe)} \quad (11)$$

where  $C_V^{MC}(Fe)$  is the vacancy concentration at the simulation box and  $C_V^{eq}(Fe)$  is the vacancy concentration at equilibrium, exponentially proportional to the vacancy formation energy. We empirically determined that, by using 0.84 eV as “effective” vacancy formation energy, by applying Eq. (11) we could get values of the same order of magnitude as in [19], and therefore directly comparable, at least in terms of trends.

Qualitatively, the AKMC results from [19] exhibit the peculiarity that the mobility increases with size, instead of decreasing, as would seem more intuitive and logical, and as consistent with the mean-field Binder–Stauffer model [37]. According to our AKMC model the mobility of the Cu precipitates decreases with size, following closely the classical Binder–Stauffer trend. This different behaviour can most likely be rationalised in terms of difference between the vacancy formation energy in bcc Cu and bcc Fe. This difference is much more pronounced in the AKMC model from [19] than in our model ( $E_V^f(Cu) = 0.82 \text{ eV}$  and  $E_V^f(Fe) = 2.20 \text{ eV}$  in [19], while in our case  $E_V^f(Cu) = 1.26 \text{ eV}$  and  $E_V^f(Fe) = 1.71 \text{ eV}$ , [26]). This makes it possible that in Soisson and Fu’s model the vacancy spends a significantly larger fraction of time inside the precipitate: the larger the precipitate, the longer. So, the possibility that the cluster migrates via surface or sub-surface hopping of the vacancy is higher than in our model.



Finally, the results shown in Fig. 7 were also obtained introducing the solubility limit of Cu atoms in the matrix. The diffusion coefficients obtained were essentially the same, except for the smaller clusters (15 and 25 atoms) at high temperature: in this case the introduction of Cu in the matrix reduced the mobility by about one order of magnitude.

#### 4. Discussion

In this section, the reliability of the above results is discussed from two viewpoints: firstly, we analyse the capability of the artificial neural network to transfer the physical information that stems out of the interatomic potential to the AKMC model without significant loss; secondly, we shortly discuss the accuracy and the limitation of the interatomic potential, necessarily taking *ab initio* data as a reference.

##### 4.1. Comparison between diffusivity results from ANN and tabulated barriers

Figs. 8 compare the dissociation energies obtained in the present work and in [24], for clusters of vacancies (upper panel) and mixed (lower panel). It can be seen that, despite the somewhat different methodology used in the two cases, the two sets of results are acceptably correlated. This suggests that, given an interatomic potential, the results are relatively robust versus the details of the way in which the energy barriers are actually estimated in the AKMC simulation.

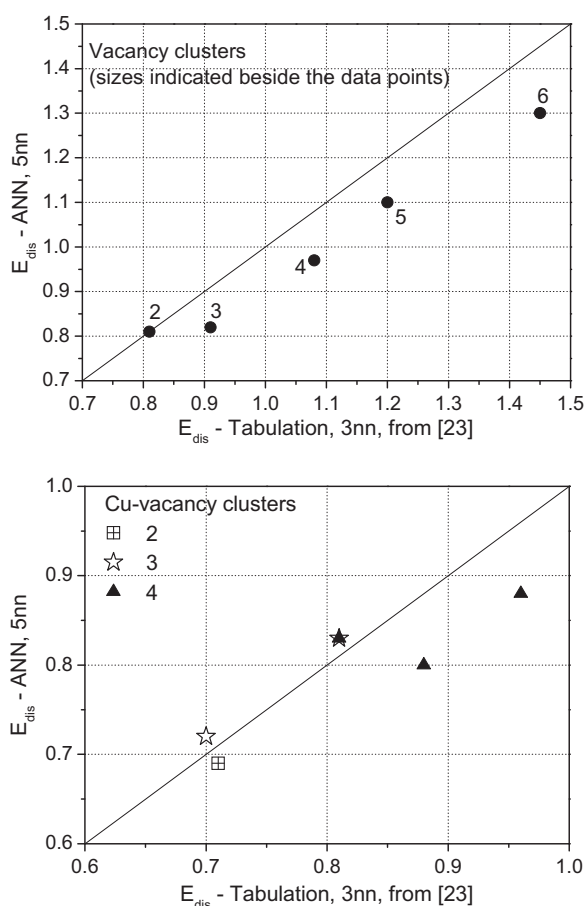


Fig. 8. Correlation between dissociation energies for vacancy clusters (above) and Cu-vacancy clusters (below) obtained with similar, yet different, methods, here ( $E_m$  - ANN results) and in [24] ( $E_m$  - Tabulation).

Next, the capability of the ANN (FeCuVac-5nn ANN) to reproduce the migration energies corresponding to the configurations encountered by the different clusters during the simulation was further tested, in the following way. A number of LAEs among those encountered were randomly extracted and the corresponding energy barrier rigorously calculated, using the NEB method. The values thereby obtained were then compared, for each cluster, with the prediction made by the ANN. The results of this comparison for all clusters are reported in [34]. Here a couple of examples of comparisons are given in Fig. 9 (upper panel), while the worst case of all is illustrated by Fig. 10. Clearly, the performance of the ANN is not the same for all clusters. This study suggests that the origin of the possible unreliability of a given ANN does not stem from the presence of a large number of defects in the LAC. Instead, it must be considered strictly as a solvable mathematical problem, related with the kind of examples (initially randomly chosen) on which the ANN is trained. Most likely, for the clusters whose energy barriers are less accurately predicted, the training set contained very few (too few) examples. The reliability of the ANN could therefore be no doubt further improved by retraining with a better selection of examples.

In order to quantify even better up to what extent errors committed by the ANN affect the prediction of the diffusion coefficient, the latter was calculated both using the ANN and the complete tabulation of NEB energy barriers, in the case of  $\text{CuV}_2$  and  $\text{CuV}_3$  (these clusters are small enough to allow the energy barriers for all possible 5nn LAEs to be calculated by NEB and tabulated; they represent average cases in terms of ANN accuracy). The results are shown in the lower panel of Fig. 9. It can be seen that the ANN error has only a negligible influence on the final result. It is thus concluded that, with the possible exception of extreme cases (such as  $\text{Cu}_3\text{V}_3$ , Fig. 10), the use of the ANN is essentially equivalent to the use of tabulations of NEB calculated barriers.

##### 4.2. Limits of the obtained values

The previous section proves that the 'filter' introduced by the ANN between the properties of the interatomic potential used for energy barrier calculations and the AKMC model is generally 'permeable' and that using the ANN is equivalent to calculating by NEB all migration energies on-the-fly, though at a greatly reduced computational cost. There are, however, two caveats.

The first one is that in our AKMC model a constant attempt frequency is assumed ( $\nu = 6 \times 10^{12} \text{ s}^{-1}$ ). In principle, this quantity is LAE-dependent, too. Given an interatomic potential the attempt frequency can be rigorously calculated for a given LAE, applying Vineyard's equation [40] and examples of calculations could be also used to train a separate ANN, specialised on attempt frequencies. The main reason to avoid this additional procedure is that small changes in the values of the migration energies, by entering an exponential function, will certainly have a much stronger impact than equally small changes in the attempt frequency (so long as these are not systematic). On the other hand, clearly the values for the jump frequencies and diffusion coefficients obtained in this work are scaled by the choice of the value of  $\nu$ .

The second caveat concerns the reliability of the interatomic potential versus the only set of data we can use for validation, i.e. *ab initio* data, given that experimental data on binding and migration energies of Cu-vacancy clusters cannot exist. The migration energies are well reproduced by the potential when compared to the *ab initio* data available at the time of the fitting [26]. In particular, the potential we used has been demonstrated to be suitable to describe the dragging of Cu atoms by migrating vacancies, contrary to other potentials [26]. However, also *ab initio* data are affected by uncertainties. Most notably, the reference *ab initio* values of binding energies used to fit the potential were different from the most

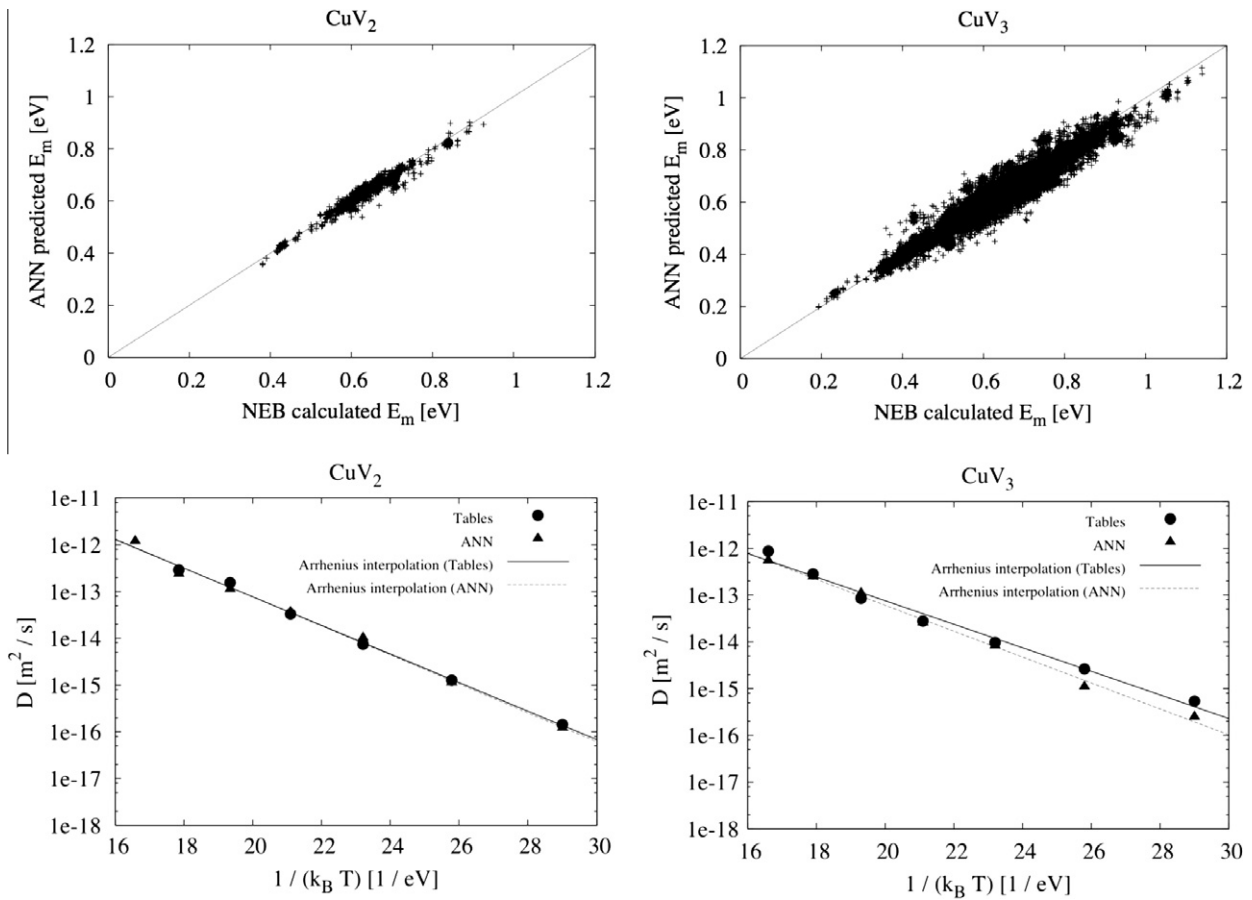


Fig. 9. Upper panel: Correlation between the migration energies predicted by the ANN and those calculated by NEB, for the two clusters CuV<sub>2</sub> and CuV<sub>3</sub> (mean errors: 1.77% for CuV<sub>2</sub>, 2.81% for CuV<sub>3</sub>). Lower panel: corresponding diffusion coefficient calculated from the complete tabulation of all possible migration energies and from the ANN.

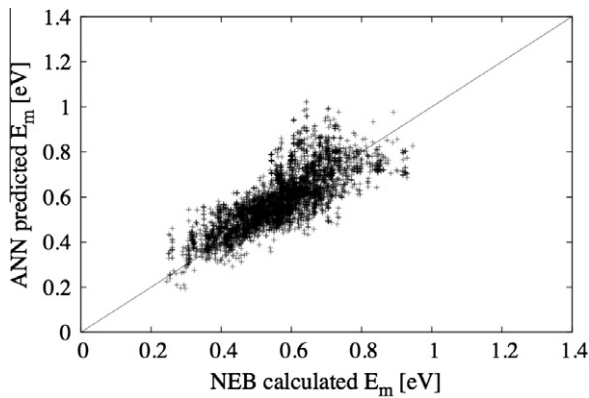


Fig. 10. Correlation between the migration energies predicted by the ANN and those calculated by NEB, in the case of the Cu<sub>3</sub>V<sub>3</sub> cluster (worst case): mean error = 11.79%, Pearson's correlation index = 0.78.

recent ones reported here. As anticipated, the comparison made in Tables 1 and 2 suggests that the Cu–vacancy binding energies are systematically underestimated by the potential. (At the same time, it should be remembered that lower binding energy values than DFT ones were needed to properly model Cu precipitation in Fe with an AKMC model, as shown in [17,20,29].) If the potential underestimates the Cu–vacancy binding energies, of all quantities calculated here, the dissociation energy and the lifetime of the clusters are the most affected and are, therefore, probably underestimated by our results. Thus, in reality these clusters might be

more strongly bound and survive for exponentially larger times before dissolving. We are any way confident that at least the trends should remain largely acceptable.

### 5. Concluding remarks

We have shown here how it is possible to rely on atomistic kinetic Monte Carlo tools, exploiting advanced computational techniques such as artificial neural networks for the prediction of vacancy migration energies as functions of the local atomic environment, to provide an assessment of the stability and mobility of mixed copper–vacancy clusters in iron. These quantities are in practice inaccessible to experiments or to molecular dynamics simulations and can alternatively be obtained only by heavy *ab initio* calculations, for a limited number of cases. The reason for studying these clusters is that they are expected to play a key role in the process of copper precipitation in iron alloys under irradiation. The mobility and stability parameters deduced in this work can so now be used to parameterize models, such as object kinetic Monte Carlo, describing the nanostructure evolution of these alloys under irradiation.

The reliability of the artificial neural network to predict the migration energy of a vacancy as a function of the local atomic environment was generally good and in some cases excellent. It has been seen that relatively poor performances are not due to inherent problems of the method, but only to the lack of proper examples on which the neural network is trained. The main limitation of the method is that, clearly, it cannot do better than the potential used to produce the examples that are provided and the

number of examples that are required is fairly large. So, at the moment, it does not seem possible to train the neural network directly on *ab initio* results, although in principle this is a possible route to follow.

### Acknowledgements

This research was partially supported by the EURATOM 7th Framework Programme, under Grant Agreement No. 232612 (Perform60 project). M.I. Pascuet acknowledges funding by the Belgian Scientific Policy Office (BelSPO), and by CONICET, Argentina.

### References

- [1] G.R. Odette, G.E. Lucas, JOM 53 (7) (2001) 18–22.
- [2] Y. Nagai, Z. Tang, M. Hassegawa, T. Kanai, M. Saneyasu, Phys. Rev. B 63 (2001) 134110.
- [3] Y. Nagai, K. Takadate, Z. Tang, H. Ohkubo, H. Sunaga, H. Takizawa, M. Hasegawa, Phys. Rev. B 67 (2003) 224202.
- [4] M. Lambrecht, L. Malerba, A. Almazouzi, J. Nucl. Mater. 378 (2008) 282.
- [5] C.S. Becquart, C. Domain, Nucl. Instrum. Methods Phys. Res. B 202 (2003) 44.
- [6] J. Marian, B.D. Wirth, G.R. Odette, J.M. Perlado, Comp. Mater. Sci. 31 (2004) 347–367.
- [7] W.M. Young, E.W. Elcock, Proc. Phys. Soc. 89 (1966) 735.
- [8] A.B. Bortz, M.H. Kalos, J.L. Lebowitz, J. Comp. Phys. 17 (1975) 10.
- [9] F. Soisson, Philos. Mag. 85 (2005) 489.
- [10] F. Soisson, J. Nucl. Mater. 349 (2006) 235.
- [11] A. Chatterjee, D.G. Vlachos, J. Computer-aided Mater. Des. 14 (2007) 253.
- [12] B.D. Wirth, G.R. Odette, Mater. Res. Soc. Symp. Proc. 540 (1999) 637.
- [13] C. Domain, C.S. Becquart, J.-C. van Duysen, Mater. Res. Soc. Symp. Proc. 540 (1999) 643.
- [14] C. Domain, C.S. Becquart, J.-C. van Duysen, Mater. Res. Soc. Symp. Proc. 650 (2001) R3.2.1–R3.2.6.
- [15] S. Schmauder, P. Binkele, Comp. Mater. Sci. 25 (2002) 174.
- [16] Y. LeBouar, F. Soisson, Phys. Rev. B 65 (2002) 094103.
- [17] E. Vincent, C.S. Becquart, C. Domain, J. Nucl. Mater. 351 (2006) 88.
- [18] E. Vincent, C.S. Becquart, C. Domain, Nucl. Instrum. Methods Phys. Res. B 255 (2007) 78.
- [19] F. Soisson, C.C. Fu, Phys. Rev. B 76 (2007) 214102.
- [20] E. Vincent, C.S. Becquart, C. Pareige, P. Pareige, C. Domain, J. Nucl. Mater. 373 (2008) 387.
- [21] C. Domain, C.S. Becquart, L. Malerba, J. Nucl. Mater. 335 (2004) 121.
- [22] Yu.N. Osestky, Def. Diff. Forum 188–190 (2001) 71.
- [23] F. Djurabekova, R. Domingos, G. Cerchiara, N. Castin, E. Vincent, L. Malerba, Nucl. Instrum. Method Phys. Res. B 255 (2007) 8.
- [24] F.G. Djurabekova, L. Malerba, C. Domain, C.S. Becquart, Nucl. Instrum. Methods Phys. Res. B 255 (2007) 47.
- [25] L. Malerba, R.C. Pasianot, SCK•CEN External Report ER-6, February 2006.
- [26] R.C. Pasianot, L. Malerba, J. Nucl. Mater. 360 (2007) 118.
- [27] N. Castin, L. Malerba, J. Chem. Phys. 132 (2010) 074507.
- [28] H. Jonsson, G. Mills, K.W. Jacobsen, in: B.J. Berne, G. Ciccotti, D.F. Coker (Eds.), Classical and quantum dynamics in condensed phase simulations, World Scientific, Singapore, 1998.
- [29] E. Vincent, PhD dissertation, University of Lille, 2006.
- [30] G. Kresse, J. Hafner, Phys. Rev. B 47 (1993) 558; *ibid.* 49 (1994) 14251.
- [31] J.P. Perdew, Y. Wang, Phys. Rev. B 45 (1991) 13244.
- [32] D. Vanderbilt, Phys. Rev. B 41 (1990) 7892; G. Kresse, J. Hafner, J. Phys.: Condens. Matter 6 (1996) 8245.
- [33] H.J. Monkhorst, J.D. Pack, Phys. Rev. B 13 (1976) 5188.
- [34] M.I. Pascuet, N. Castin, L. Malerba, SCK•CEN External Report ER-93, May 2009.
- [35] M.W. Guinan, R.N. Stuart, R.J. Borg, Phys. Rev. B 15 (1977) 699.
- [36] P.G. Shewmon, Diffusion in Solids, McGraw Hill, 1963 (Chapter 2).
- [37] K. Binder, D. Stauffer, J. Stat. Phys. 6 (1972) 49.
- [38] K. Binder, M.H. Kalos, J. Stat. Phys. 22 (1972) 363.
- [39] K. Binder, D. Stauffer, Phys. Rev. Lett. 33 (1974) 1006.
- [40] G.H. Vineyard, J. Chem. Phys. Sol. 3 (1957) 121.